Track of fluid paleocirculation in dolomite host rock at regional scale by the Anisotropy of Magnetic Susceptibility (AMS): An example from Aptian carbonates of La Florida (Northern Spain)

Mourad Essalhi, Stanislas Sizaret, Luc Barbanson, Yan Chen, Yannick Branquet, Dominique Panis, Pierre Camps, Pierre Rochette, Angels Canals

Track of fluid paleocirculation in dolomite host rock at regional scale by the Anisotropy of Magnetic Susceptibility (AMS): An example from Aptian carbonates of La Florida (Northern Spain)

Mourad Essalhi[1]*, Stanislas Sizaret[1], Luc Barbanson[1], Yan Chen[1], Yannick Branquet[1], Dominique Panis[1], Pierre Camps[2], Pierre Rochette[3] and Angels Canals[4]

[1] ISTO, CNRS–Université d'Orléans. 1A, rue de la Férollerie 45071 Orléans Cedex 2, France

[2] CNRS–Université Montpellier 2, 34095 Montpellier cedex 5, France

[3] CEREGE, Université Aix Marseille–CNRS, Europôle de l'Arbois, BP 80 13545, Aix En Provence, France

[4] Dpt. Cristalografia, Mineralogia i Deposits minerals, Universitat de Barcelona 08028, Spain

* Corresponding author, e-mail address: mourad.essalhi@univ-orleans.fr

Phone: 0033238494652

Fax: 0033238417308

Abstract

The present study aims to apply the AMS method (Anisotropy of Magnetic Susceptibility) at a regional scale to track the fluid circulation direction that has produced an iron metasomatism within pre-existing dolomite host rock. The Urgonian formations hosting the Zn-Pb mineralizations in La Florida (Cantabria, northern Spain) have been taken as target

for this purpose. Sampling was carried out, in addition to ferroan dolomite host rock enclosing the Zn-Pb mineralizations, in dolomite host rock and limestone to make the comparison possible between magnetic signals from mineralized rocks, where fluid circulation occurred, and their surrounding formations. AMS study was coupled with petrofabric analysis carried out by texture goniometry, Scanning Electron Microscopy (SEM) observations and also Shape Preferred Orientation (SPO) statistics. SEM observations of ferroan dolomite host rock illustrate both bright and dark grey ribbons corresponding respectively to Fe enriched and pure dolomites. SPO statistics applied on four images from ferroan dolomite host rock give a well defined orientation of ribbons related to the intermediate axis of magnetic susceptibility K_2. For AMS data, two magnetic fabrics are observed. The first one is observed in ferroan dolomite host rock and characterised by a prolate ellipsoid of magnetic susceptibility with a vertical magnetic lineation. The magnetic susceptibility carrier is Fe-rich dolomite. These features are probably acquired during metasomatic fluid circulations. In Fe-rich dolomite host rock, ‹c› axes are vertical. As a rule, (0001) planes (i.e. planes perpendicular to ‹c› axes) are isotropic with respect to crystallographic properties. So, the magnetic anisotropy measured in this plane should reflect crystallographic modification due to fluid circulation. This is confirmed by the texture observed using the SEM. Consequently, AMS results show a dominant NE-SW elongation interpreted as the global circulation direction and a NW-SE secondary elongation that we have considered as sinuosities of the fluid trajectory. The second type of magnetic fabric is essentially observed in the limestone and characterised by an oblate form of the ellipsoid of magnetic susceptibility, a horizontal magnetic foliation and mixed magnetic susceptibility carriers. It is interpreted as a sedimentary fabric.

Key words: AMS, carbonates, fluid flow, growth anisotropy, mineral texture.

1. Introduction

Tracking hydrothermal circulation is one of the main challenges in investigations of metasomatism. Classic studies have used geochemical signature and megascopic hydrodynamic models (e.g., Wing and Ferry, 2007). However, in these models fluid paths are not constrained by field observations. The method of Anisotropy of Magnetic Susceptibility (AMS) has been proposed to track flow circulation (Hounslow, 2001; Sizaret et al., 2001, 2003, 2006a; De Wall and Warr, 2004). This approach is based on crystal growth orientations (Kessler et al., 1972) and supported by the crystal growth theory (Prieto et al., 1996; Sizaret et al., 2006b). These studies show a higher growth rate on crystal faces in upstream position which produces crystal elongation parallel to the direction of circulation. The orientation of this elongation can be measured using AMS method, and interpreted in terms of flow direction.

AMS, considerably developed in the last 30 years, was for a long time devoted to structural and rock petrofabric studies (e.g., Hrouda, 1982; Tarling and Hrouda, 1993; Ferré, 2002), to granite pluton characterization (e.g., Jover et al., 1989; Bouillin et al., 1993; Talbot et al., 2005) or magmatic flow description (e.g., Nomade et al., 2000), and to describe the rock deformation (e.g., Borradaile and Tarling, 1981; Evans et al., 2003). This technique is based on the directional variation of the magnetic susceptibility K on sample scale. The latter is a property of solids reflecting the capacity of a material to be magnetized in a given magnetic field ($K = M/H$, M and H are respectively the induced and applied magnetic fields). In an anisotropic material, K can be described as a second rank tensor or an ellipsoid defined by three perpendicular oriented axes K_1, K_2 and K_3 (the maximum, intermediate and minimum of the magnetic susceptibility, respectively). K_1 and K_3 are respectively considered as the magnetic lineation and the pole of the magnetic foliation.

Several studies were carried out on the relation between carbonate single crystals and their magnetic susceptibility (Owens and Rutter, 1978; Rochette, 1988; Shogenova, 1999; Schmidt et al., 2006). In carbonates, magnetic susceptibility is controlled by intrinsic properties (such as crystallographic directions and chemical composition) and crystal shape. So, a fluid migration occurring in these rocks and producing recrystallisation and/or cementation would introduce a modification in composition and/or shape of their constitutive minerals and, therefore, a remarkable variation of the magnetic fabrics. The latter can be measured and interpreted to infer the characteristics of circulating paleo-fluid (Prieto et al., 1996; Sizaret et al., 2006b). As observed by Kessler et al. (1972) and modelled by Sizaret et al. (2006b), this fluid circulation may be evidenced by a growth anisotropy. According to these authors, the thickest growth bands show the upstream, whereas the thinnest ones indicate the downstream of the flow. These results are fundamental to recognize the relationship between the carbonate crystal growth and their magnetic fabrics.

The main objective of this study is to link AMS data and mineral texture analysis to fluid migration in a carbonate environment, at a larger regional scale with respect to previous works (Sizaret et al., 2003, 2006a). For this work it has been chosen to apply the method to study deposit in carbonate environment where large fluid migration is suspected.

The Zn-Pb mineralizations of Cantabrian mining district are located in Cretaceous basin with occurrence of salt dome (Fig. 1A). The ore is hosted in Urgonian carbonates and is associated with epigenetic dolomite (Barbanson et al., 1983; Barbanson and Touray, 1987; Barbanson, 1993). Recent study based on Br, Cl and Na concentration of the mineralising fluids suggest a general mixing involving halite saturated brine derived from halite dissolution suggesting a strong link with salt dome (Grandia et al., 2003). At La Florida mine this relation is also supported by a geochromatography of Organic matter suggesting migration from salt

into the Urgonian plate form (Hu et al., 1995; 1998). Tracking mineralising flow direction on this site using the method based on AMS and texture analysis is the challenge of this paper.

2. Geological setting

2.1. General framework

The Zn-Pb mine of La Florida (Province of Santander, Spain) is located in the western part of a Cretaceous basin, which overlies the Asturian Paleozoic massif in the west and the Basque massif in the east (Fig. 1B). This basin is covered by the Vieja Castilla and the Ebro Tertiary deposits in its south and limited by the Bay of Biscay in its north. The meridian line of Santander forms a rough limit between an oriental domain more intensely folded during the Pyrenean orogeny and a west-Santanderian domain where this orogeny is weakly expressed. This latter domain contains the La Florida mine where this study has been carried out. The eastern border of this mine is limited by Triassic evaporite diapirs (Fig. 1B).

Fig. 1

The geological history of this basin starts at the Aptian and the Albian when a distensive folding of the Basco-Cantabric unit induces the development of a passive continental margin (Rat, 1982; Rat and Pascal, 1982). This event initiates the development of large Urgonian carbonate platforms in the west-Santanderian domain. Pascal (1982, 1984) described the evolution of this Urgonian complex as the succession in time of three bio-sedimentary systems. The first two systems end up respectively by the lower and the upper rudist Urgonian platforms (Fig. 2A). The last bio-sedimentary system is characterised by an invasion of the basin by terrigenous sediments.

2.2. Metallogenic framework

La Florida Pb-Zn mine is located close to the well known Reocin mine (60 MT, 8% Zn) in the western part of the Santander district in the Aptian Basque-Cantabrian basin. In this

district a number of similarities between Urgonian hosted Zn-Pb deposits of Cantabria allowed Barbanson and Touray (1987) to define a "west-Santanderian" sphalerite – galena ore deposit type in carbonated environment. Three main characteristics are common in these deposits: (i) mineralizations are located in ferroan dolomite host rock (Fig. 2A), (ii) these mineralizations occur mainly close to the synsedimentary faults controlling the Urgonian sedimentation, and (iii) in the ore, the paragenetic succession is split in two main mineralogical sequences: sphalerite – galena – Fe-rich dolomite and dolomite – marcasite (Fig. 2B). Geological observations suggest that synsedimentary and epigenetic mineralizations were formed during an Aptian-Early Cenomanian metallogenic epoch. It could be noted that ferroan dolomite host rock is affected by an Aptian emersion (Barbanson, 1993). Barbanson and Touray (1987) recognize two genetic processes forming deposits of Cantabria (La Florida and other mining districts); the first is interpreted as a synsedimentary mineralization occurring in paleo-channels, whereas the second is an epigenetic mineralization observed in subterranean cavities. In both cases mineralizations display the same paragenetic succession as presented in figure 2B.

Fig. 2

In the Cantabria district two main stages of dolomitization could be described. The first one consists in pervasive dolomitization affecting the Aptian limestone. The analysis of the $\delta^{13}C_{PDB}$ and $\delta^{18}O_{SMOW}$ on dolomite host rock of the Reocin deposit are interpreted by Velasco et al. (2003) as *"the result of the early circulation of hot Mg^{2+} -rich fluids probably derived from the dewatering of basinal mudrocks"*. The second stage is dominated by a main iron rich dolomitization and the third stage corresponds to the saddle dolomite and Fe-dolomite crystals present in the ore. The mineralizing fluids have been studied and the homogenisation temperature measured in sphalerite of the Reocin mine is about 77°C, with a salinity of 25.5 wt percent NaCl equiv (Grandia et al., 2003). Moreover, analysis of Na, Cl and Br contents in fluid inclusion of sphalerite and dolomite associated to sphalerite at La

Florida and Reocin compared with other data measured in the mineralisation of the Basque-Cantabrian Basin suggest a precipitation by mixing of two fluids. *"One of the end members could have been a highly evaporated brine and the second fluid could have been either an evaporated brine was not halite saturated or a diluted halite dissolution brine"* (Grandia et al. 2003).

At La Florida, Zn-Pb mineralizations are strictly associated with the ferroan dolomite host rock, which is enclosed in ordinary dolomite host rock, and the whole is involved in the Aptian limestone (Fig. 2A; Barbanson et al., 1983; Velasco et al., 2003). Organic matter studies related to the mineralizations showed a geochromatographic fractionation toward West, which is more coherent with an epigenetic origin of mineralizations (Hu et al., 1995, 1998). To track paleocirculation linked to dolomitization, the study is focus on the surrounding rocks with three types of simple mineralogical assemblage; Aptian biomicritic limestone locally dolomitized is constituted by calcite, whereas dolomite host rock and ferroan dolomite host rock are composed by anhedral crystals of dolomite and Fe-rich dolomite, respectively (Fig. 2B). Iron oxides are generally rare in limestone and dolomite host rock and are relatively more abundant in ferroan dolomite host rock (SEM observations).

2.3. Field structural observations

Pyrenean orogeny deformation is weakly marked in the studied zone by scarce styloliths and a few kilometer-scale folds. On the outcrop scale, the synsedimentary deformation is documented by NW-SE tilting that accommodates organic matter deposition. An observed hydroplastic slickenside lineation with direction of N110° reflects a deformation type developed in partially lithified sediments. Concerning the syndolomitization deformation, it appears in some N30° subvertical veins which are filled with baroque dolomite associated to the Zn-Pb mineralizations.

3. Textural analysis

3.1. Lattice Preferred Orientation

To better understand the relationship between crystallographic axis orientations of carbonates and their corresponding magnetic fabrics, measurements of lattice preferred orientation were realized by the Universal Goniometer UG 950 (Inel) on two dolomite host rock and two ferroan dolomite host rock samples to ensure representative results. The method is described by Schultz (1949a, 1949b). The spatial orientations of a (h k i l) diffracting plane may be defined by records of X-rays diffracted by the rotating sample along two orthogonal axes. A spatial statistical analysis allows to infer the crystallographic preferential orientation. Datum acquisition and treatment were described in Heizmann et al. (1988). To facilitate comparison and interpretation all samples were prepared according to their magnetic responses (i.e. in the K_1K_2 or K_2K_3 planes). All measurements were done with collimator window of 1x1 mm^2; sample was moved by steps on 15 mm. The (0006) diffraction peak was chosen because (i) the relation with ‹c› axes is trivial and (ii) in the diffractogram, the neighbouring of (0006) line is free of other diffraction peaks preventing overlapping by other diffraction lines.

Fig. 3 shows the measurements of lattice preferred orientation on all 4 dolomite host rock and ferroan dolomite host rock samples in tilt-corrected coordinates. We note that the ‹c› axes in dolomite host rock (Figs. 3A and B) and ferroan dolomite host rock (Figs. 3C and D) are well identified and grouped in a vertical position.

Fig. 3

3.2. SPO statistics and growth bands studies in the (0001) isotropic plane

Thin sections from the same samples studied by texture goniometry were observed by Scanning Electron Microscope (SEM), to examine their mineralogical compositions and to

study the geometry of carbonate growth bands in the "isotropic" plane perpendicular to the ‹c› axes. Representative SEM images from studied thin sections are presented in Fig. 4.

In ferroan dolomite host rock we note the presence of two types of elongated ribbons whose limits cut across grain boundary (Fig. 4A). Within single crystal grains of Fe-rich dolomite two zones can be frequently distinguished: a pure dolomitic one hosting dark inclusions probably argillaceous and a Fe-dolomitic free of inclusions. The dark ribbons are made up of $CaMg(CO_3)_2$ whereas the bright ones are $Ca(Mg,Fe)(CO_3)_2$ in composition. Dark zones composed solely by pure dolomite correspond to the relic of initial rock (i.e. dolomite host rock). This difference between the two types of ribbons reflects a chemical flow that induced enrichment of some dolomite crystal zones by iron. To quantify the mean orientation of ribbons elongation, shape preferred orientation statistics (Launeau and Robin, 1996) has been carried out on microscopic images of a thin section. Results of image analysis are presented in Fig. 4B. The statistics were realized on four backscattered images taken in different places of the thin section; they give almost the same mean orientation. The result shows a well defined ENE-WSW elongation with a shape factor R of 1.387. The "nearest neighbor" statistics were also done with the same program on the relic of dolomite, they show an alignment according to the ENE-WSW direction with a shape factor R of 1.11 (Fig. 4C).

Fig. 4

For dolomite host rock one note the presence of growth bands around triangular sections (i.e. isotropic plane) of single dolomite crystals (Figs. 4D and E). As shown by punctual analysis, the difference in grey intensities between the growth bands is due to slight departure from stoechiometry: clear grey and dark grey bands are respectively richer in Ca and Mg. The difference in composition is thus noticed on scale of individual crystals of dolomite. The observed thickness variation in individual band outlines the anisotropy growth due to external media.

4. Magnetic analysis

Three hundreds and twenty-seven AMS oriented cores of thirty-four sites have been drilled in limestone, dolomite host rock and ferroan dolomite host rock located along four lateral transects on the northern flank of an E-W oriented anticline (Fig. 2A). This sampling scheme allows to compare the magnetic signals between mineralised rocks where fluid circulation occurred and their surrounding formations, and also to recognize spatial variation of the magnetic signal of each lithology. Sampling and measurement methods are described in Tarling and Hrouda (1993). Four oriented cores were at least taken from each site by a portable gasoline drill.

4.1. Magnetic Behaviour of carbonates

It is well known that the magnetic susceptibility of carbonates is mainly controlled by the orientation of their crystallographic axes (e.g Nye, 1961). Studied carbonates display trigonal symmetry and the crystallographic cell can be described by four crystallographic axes. Three coplanar axes ‹a›, ‹b› and ‹t› are oriented at 120° each one to other, and the fourth axis ‹c› is perpendicular to the three formers. The four axes are such that ‹a› = ‹b› = ‹t› ≠ ‹c›. The latter is parallel to the 3-fold axis of symmetry. In the case of a perfect single crystal of calcite for example, the absolute value of the magnetic susceptibility along the ‹c› axis is higher than those along the ‹a›, ‹b› and ‹t› axes, which have the same magnetic susceptibility (K_c = -1.38 x 10^{-5} [SI], $K_a = K_b = K_t$ = -1.24 x 10^{-5} [SI], after the “International Critical Tables” in Nye, 1961). So, as it could be predicted from Neumann principle in terms of magnetic susceptibility, calcite and other trigonal carbonates are isotropic according to the (0001) plane containing ‹a›, ‹b› and ‹t› axes.

On the other hand, the anisotropy of magnetic susceptibility in carbonates was the subject of several studies (Owens and Rutter, 1978; Rochette, 1988; Hrouda, 2004; Schneider et al., 2004; Schmidt et al., 2006). AMS is controlled by the orientation of their crystallographic axes, their chemistry as well as the preferential orientation of their constitutive grains. According to Schmidt et al. (2006), the ‹c› axes are parallel to K_3 axis (inverse fabric) in low iron-bearing carbonates (note that K_1, K_2 and K_3 are classified according to their algebraic values, Hrouda, 1982). So, in trigonal diamagnetic carbonates as calcite and pure dolomite, the lower value of K is parallel to the ‹c› axis. In rich iron-bearing carbonates they are rather parallel to the K_1 axis (normal fabric). These behaviours are observed in our samples; as shown by the comparison between lattice preferred orientation measurements obtained by texture goniometry and AMS results performed on the same samples (Fig. 3). In Fe-poor dolomite host rock, the ‹c› axes are very well grouped and they are oriented parallel to the K_3 axis of the magnetic ellipsoid (Figs. 3A and B), while in ferroan dolomite host rock, they are also vertical but parallel to K_1 axis (Figs. 3C and D). This behaviour indicates hence that iron amount in carbonates controls their magnetic response.

4.2. Magnetic mineralogical identification

In addition to microscopic observations described above, four other methods were used to identify the magnetic susceptibility carrier(s) in studied rocks: bulk susceptibility measurement (KLY-3S Kappabridge apparatus at the Institut des Sciences de la Terre d'Orléans, ISTO), Isothermal Remanent Magnetization (IRM, JR-5A automatic spinner magnetometer, ISTO), magnetic hysteresis curves (Vibrating Sample Magnetometer (VMS), Princeton Measurements Model 3900, Southern Illinois University; VMS of CEREGE; and inductometer within an electro-magnet at the Institut de Physique du Globe de Paris, IPGP)

and Anisotropy of Remanent Magnetization (ARM, 2G cryogenic SQUID magnetometer with an AF demagnetizer at the University of Montpellier).

Bulk susceptibility intervals for each lithology are plotted in Fig. 5A. A majority of limestone samples have low and negative magnetic susceptibilities; they contain thus principally diamagnetic minerals, but some samples show rather positive susceptibilities suggesting the presence of small quantities of para- and/or ferromagnetic (s.l.) minerals. The dolomite host rock and ferroan dolomite host rock samples have relatively low but positive magnetic susceptibilities; in this case the rocks are mainly constituted of paramagnetic minerals, with probably a small amount of ferromagnetic (s.l.) minerals.

Fig. 5

Isothermal Remanent Magnetization (IRM) acquisition was carried out on one sample of each lithology: limestone (site L_3), dolomite host rock (D_4) and ferroan dolomite host rock (FD_2) (see Fig. 2A). Results illustrate that IRM of limestone shows a fast and total magnetic saturation for applied field values of 180 mT (Fig. 6A). This saturation value indicates a low coercivity ferromagnetic (s.l.) component which illustrates the presence of magnetite (Dunlop and Özdemir, 1997). For dolomite host rock (Fig. 6B) and ferroan dolomite host rock (Fig. 6C) we note, in addition to the low coercivity component corresponding to magnetite, a high coercivity component shown by a quasi linear increase of magnetization. That magnetic behaviour illustrates a probable existence of hematite or goethite with higher coercivities (Dunlop and Özdemir, 1997). It should be noted that values of remanent magnetization are very low (few $mA.m^{-1}$); consequently, the quantity of ferromagnetic (s.l.) minerals is very weak in all studied samples.

The hysteresis measurements were done on samples coming from the same sites studied by IRM measurements, three apparatus with different precisions were used and give similar results, the most representative are showed in Fig. 6. The hysteresis curves are not perfectly

linear for all lithologies and they show a strong dominance of para-, dia- and antiferromagnetic fractions component in comparison with the hysteretic ferrimagnetic one. The limestone curve has a negative slope (Fig. 6D); K is therefore negative and the main magnetic susceptibility carrier is a mixture between diamagnetic and ferromagnetic (s.l.) as seen before (Fig. 5A). Pure and ferroan dolomite host rock curves have a positive slope, signifying that K is positive and that the magnetic carriers in these rocks are mainly a mixture between paramagnetic and ferromagnetic (s.l.) minerals (Figs. 6E and 6F). Saturation determined on the corrected curves, is reached at about 500-600 mT. At 180 mT (saturation value of magnetite), we have about 75% of saturation for limestone, 60% for dolomite host rock and about 55% for ferroan dolomite host rock. This result indicates that the ferromagnetic (s.l.) contribution is a mixture between minerals with soft and hard coercivities (magnetite and hematite/goethite, respectively).

Fig. 6

Although the bulk susceptibility histogram (Fig. 5A) show a dominance of dia- and paramagnetic minerals in limestone and dolomites host rocks, respectively, but iron oxides were detected by microscopic observations, and contribution of ferromagnetic (s.l.) minerals is identified by IRM and hysteresis measurements. In limestone the IRM measurements show that the unique ferromagnetic mineral is the magnetite (Fig. 6A) but hysteresis ones suggest rather a mixture between magnetite and hematite/goethite (Fig. 6D). In the dolomite and ferroan dolomite host rocks, IRM (Figs. 6B and 6C, respectively) and hysteresis (Figs. 6E and 6F, respectively) curves show also a mixture between magnetite and hematite. However, it is very difficult to estimate the exact amount of each of them, because the overall hysteresis loop of bi-mineral mixture does not represent a simple sum of contributions corresponding to individual components, but is affected by interactions between magnetite and hematite grains (Hejda et al. 1994). On the other hand, M_{rs}/M_s values in dolomite host rock (0.043) and ferroan dolomite host rock (0.19) indicate that there is a dominance of magnetite (Peters and

Thompson, 1998). An over-estimation of the magnetite component in studied carbonates is possible by using the saturation remanence Mrs. Thus; saturation remanence M_{rs} is proportional to the magnetite concentration. Considering the M_{rs} value of magnetite $M_{rs} \geq 10.A.m^2 / Kg$, its amount in limestone, dolomite and ferroan dolomite host rocks is estimated below 2.1, 1.2 and 9.7 ppm, respectively. Considering these quantities of ferromagnetic minerals in studied samples and the magnetic susceptibility reported in the literature (Rochette et al., 1992), the ferromagnetic minerals contribution to the magnetic susceptibility appears to be low. This is obvious for ferroan dolomite host rock that has a strong magnetic susceptibility. This point will be completed by the comparison of Anisotropy of Remanent Magnetization (ARM) and AMS measurements.

The possible existence of mixed fabrics (i.e. between dia and/or para and ferromagnetic (s.l.) minerals) should be clarified. The magnetic susceptibility carriers seem to be difficult to identify, so ARM measurements were carried out on samples of limestone (from site L_{10}), dolomite host rock (D_2) and ferroan dolomite host rock (FD_3). Measurements were carried out in three steps; (i) demagnetization of the sample with an alternating field (AF = 160 mT), (ii) ARM acquisition with a bias direct field of 250 μT (and AF = 150 mT), (iii) measurement of the induced ARM values. These three steps are repeated for 9 positions. The remanent anisotropy is modelled by ellipsoid constructed from the axial measurements plus the off-axis remanence terms. In Fig. 7 are presented stereograms showing the relation between the orientation of ARM ellipsoid axes and the AMS ones. The dolomite host rock presents the same fabrics between ARM and AMS indicating thus that susceptibility carrier is mixed with contribution of ferromagnetic minerals (s.l.) and dia/paramagnetic ones in the magnetic fabric of dolomite host rock (Fig. 7B). For the ferroan dolomite host rock, the stereogram shows a significant difference between ARM and AMS, so the susceptibility magnetic carrier should not be ferromagnetic (s.l.) minerals but a paramagnetic one (Fig. 7C). In limestone, ARM and

AMS ellipsoid axes orientation are comparable, though it is less obvious than in dolomite host rock (Fig. 7A), the carrier is probably a mixture between diamagnetic and ferromagnetic (s.l.) minerals (and perhaps paramagnetic ones).

Fig. 7

According to above laboratory analyses on rock magnetism we conclude that the magnetic susceptibility carrier is paramagnetic carbonates (Fe-rich dolomite) in ferroan dolomite host rock and mixture between iron oxides (magnetite often) and carbonates (dolomite and calcite, respectively) in dolomite host rock and limestone.

4.3. Magnetic fabrics

The AMS measurements were carried out by KLY-3S kappabridge. For each site, the mean orientation of the principal axes of the ellipsoid of magnetic susceptibility is calculated by the "bivariate statistics" (Henry and Le Goff, 1995). Principal susceptibility axes and AMS parameters are calculated by SUSAR program (AGICO).

For diamagnetic minerals, Hrouda (2004) propose two models to explain the AMS signal for quartzite/evaporite and marble/limestone. He suggest the use of signed values (approach 1) for plotting principal directions and absolute values of K_1, K_2 and K_3 (approach 2) to calculate T parameter in case of marble or limestone, because it is calculated from <c> axes distribution pattern (in opposite to the quartzite/evaporite model which propose to use the T parameter based on the signed principal susceptibilities (approach 1), because it describes the shape of the susceptibility ellipsoid of the ferro-/paramagnetic admixture fraction). This is the case here since SUSAR program used in our measurements utilizes signed negative values (approach 1) for plotting principal directions and absolute values (approach 2) for calculating all AMS parameters.

Table 1 resumes the AMS data with their principal associated parameters and Fig. 5B shows a plot of the shape parameter (T) versus the corrected anisotropy degree (P') for the three studied lithologies. P' for diamagnetic samples has been calculated following the equation given in Table 1.

To limestone, the shape parameter T is mainly positive; the ellipsoid of magnetic susceptibility presents an oblate shape. A remarkable high P' values has been observed (Table 1 and group Y of Fig. 5B), however, this may be an artefact generated by an overlap of diamagnetic and paramagnetic susceptibilities. Hrouda (1986) has shown by an AMS study on quartzites that the interference of dia- and paramagnetic behaviours can bias anisotropy results and change P' values for certain susceptibility ranges. This phenomenon characterizes our samples as shown by Fig. 5C, the corrected anisotropy factor (P') versus bulk susceptibility (K_v). A fast increase of P' occurs when K_v is close to 0. In this case, high P' values are not related to deformation and thus we consider that the AMS of limestone is characterised by oblate ellipsoid and probably low anisotropy. As limestone, the ordinary dolomite host rock show an oblate ellipsoid of AMS with a low anisotropy degree P' suggesting the absence of significant deformation (Table 1 and group X of Fig. 5B) (Tarling and Hrouda, 1993). The ellipsoids of ferroan dolomite host rock sites are well distinct, the anisotropy degree P' is low ranging from 1.002 to 1.012 and the shape parameter T is negative; the magnetic fabrics are thus dominated by linear texture (Table 1 and group Z of Fig. 5B) (Tarling and Hrouda, 1993). This prolate shape of the ellipsoid of magnetic susceptibility characterizes the fabrics inherited from Fe-metasomatism. This process may be the principal cause to make a distinguishable difference on the magnetic fabrics between limestone-dolomite host rock and ferroan dolomite host rock due to the fluid migration in the later one.

Table. 1

Fig. 8 presents the stereographic projections of AMS measurements in tilt-corrected coordinates. In ferroan dolomite host rock, the magnetic lineation is well defined and mainly in vertical position (e.g., Figs. 8A-a, h and m), except for the site FD_{16} showing a horizontal lineation (Fig. 8A-p) and a surprising positive value of the shape parameter T. All limestone sites show horizontal magnetic lineations dominated by a NW-SE orientated direction, coherent to the deposit direction mentioned previously (e.g., Figs. 8B-b, c and j). Horizontal magnetic lineation and oblate ellipsoid suggest a sedimentary fabric for the limestone. Concerning the dolomite host rock, the AMS signals are more complicated. The orientations of magnetic fabrics are scatter and seem to be intermediate between limestone and ferroan dolomite host rock. This may be due to the mixture of ferromagnetic and paramagnetic minerals and the observed results may depend on the amount of ferromagnetic minerals in the paramagnetic matrix.

Fig. 8

5. Discussions

The AMS results show a significant difference between the surrounding rocks (limestone-dolomite host rock) and ferroan dolomite host rock. Two main fabrics could be characterized and associated each one to a geological genetic process: sedimentary and metasomatic.

The fabric observed in limestone is characterised by an oblate shape with a horizontal magnetic lineation. In dolomite host rock, scatter fabrics may be result from mixed magnetic minerals between carbonates and magnetite. The fabric occurring in ferroan dolomite host rock shows a prolate ellipsoid of magnetic susceptibility with a vertical magnetic lineation,

The sedimentary fabric is observed in limestone, but the magnetic response is complex as the susceptibility carrier is a mixture between para and ferromagnetic (s.l.) minerals (Fig.

7A). This fabric corresponds to an oblate ellipsoid of magnetic susceptibility (Fig. 5B) with a horizontal magnetic lineation (e.g., Figs. 8B-h and j). Moreover, six sites of limestone display a well defined NW-SE magnetic lineation (e.g., Figs. 8B-c and i), that is coherent with the NW-SE sedimentary transport direction (N110°) observed on outcrop (see part 2.3.) (Fig. 9). In dolomite host rock, the influence of fluid circulation is evidenced by the existence of anisotropic growth bands (Figs. 4D and E), however, the magnetic signal is difficult to interpret because of the variations of the magnetic susceptibility carriers and, particularly, of the amount of ferromagnetic (s.l.) minerals as shown by IRM, magnetic hysteresis and ARM results (Figs. 6B, F and 7B, respectively).

As discussed in Part 4.1, the absolute value of magnetic susceptibility in carbonates is more important according to ‹c› axis and it is relatively weak in the (0001) plane. According to the texture goniometry analysis, the relation between lattice preferred orientation is now well constrained; in ferroan dolomite host rock, results show a well defined correspondence between K_1 and ‹c› axes (Figs. 3C and D) with a vertical position (e.g., Figs. 8A-c, g and o). The symmetry breakdown recorded by the crystal is revealed in the K_2-K_3 "isotropic" plane. Only one site does not show the same feature as described above and has a horizontal magnetic lineation (Fig. 8A-p); this site is also the unique one to show an oblate shape of the ellipsoid of magnetic susceptibility. This abnormal behaviour is very likely due to a mixture between para- and ferromagnetic minerals, probably including diamagnetic as well.

At millimetric scale, in ferroan dolomite host rock two zones are distinguished by SEM observations: dark grey ribbons corresponding to the relic of initial rock and clear grey ribbons indicating the enrichment of iron (Fig. 4A) (see Barbanson et al., 1983). The difference in mineralogical composition reflects a chemical flux which enriched dolomite crystals by iron. These ribbons show well developed elongations and, according to SPO

statistics, their orientations present a direction parallel to the intermediate axis of magnetic susceptibility K_2 (Fig. 4B). The "nearest neighbor" statistics show also an alignment slightly parallel to the K_2 axis (Fig. 4C). This orientation may be therefore considered as the fluid flow direction (e.g., Figs. 8A-d and h), K_1 showing the ‹c› axes orientation.

If we take texture analysis and AMS results into account, we can discriminate two circulation directions; the dominant NE-SW direction interpreted as the principal direction of the fluid circulation (e.g., Figs. 8A-c, d and h), and the secondary NW-SE direction corresponding probably to the bend of fluid trajectory (e.g., Figs. 8A-g and k). Statistically, the principal direction is well observed when we plot all AMS data of ferroan dolomite host rock in the same stereogram (Fig. 8A-q). AMS data allows thus to define indirectly the fluid flow direction.

The dominant NE-SW direction of fluid circulation obtained from this study may be interpreted as the consequence of metasomatic process probably related to diapirs underlying the eastern boundary of La Florida mining district (Figs. 1 and 9). Previous geologic studies have illustrated the spatial and contemporal relations between the diapiric structures and mineralizations (Barbanson et al., 1983; Barbanson and Touray, 1987; Barbanson, 1993; Grandia et al., 2003). So, we consider the metasomatic flow as responsible to the ferriferous metasomatism of the Urgonian carbonates. Moreover, as the mineralizations are associated in time and space with ferroan dolomite host rock, we conclude that the well defined principal direction corresponds to that of the mineralizing fluid. The block-diagram presented in Fig. 9 synthesises AMS observations and geological understanding.

Fig. 9

6. Conclusion

Flow direction of metasomatic process could be tracked by magnetic fabrics. However, the reasonable AMS interpretation in carbonate depends on the good understanding on the magnetic mineralogical composition and the correspondence between the lattice preferred orientation and the principal axes of magnetic susceptibility. The textural analysis is necessary to interpret magnetic signature of fluid flow. Coupled with texture goniometry and SEM observations as well as SPO statistics, the magnetic fabric study shows a significant difference between ferroan dolomite host rock hosting the Zn-Pb mineralizations and its surrounding rocks; a dominance of the NE-SW elongation deduced from K_2 magnetic axis in ferroan dolomite host rock is interpreted as the direction of fluid migration in studied Urgonian carbonates, and this regional-scale study enhances also a comprehensive understanding on the metasomatic process in the La Florida mining district. Therefore, coupling with textural analysis, AMS method can be considered as an efficient tool to track flow in metasomatic formations at a regional scale, even if the magnetic signal is low as in studied carbonates.

Acknowledgements

We thank the EGIDE program (PAI Programme Picasso n°10998VL) for its financial support. The first author benefits a scholarship grant from the French Minister of Education and Research. The authors would like to thank the Editor C. Jaupart and the three anonymous reviewers whose comments help to improve greatly this manuscript.

References

Barbanson, L., 1993. The carbonate hosted Zn-Pb deposit of West–Santanderin type (North of Spain): Tectonical control at regional and local scale, in: Leach, D., Macquar, J., De

Marsily, G., Rouvier, H., Thibieroz, J. (Eds.), Mississippi valley type deposits in Europe and North Africa, comparisons with North American deposits, constraints on modelling paleocirculations. Proceeding Workshop MVT, Paris, pp. 15-27.

Barbanson, L., Touray, J.C., 1987. Les minéralisations Zn-Pb des systèmes biosédimentaires urgoniens du domaine Ouest-Santandérin (Nord de l'Espagne), in: Pelissonnier, K., Sureon, J. (Eds.), Mobilité et concentration des métaux de base dans les couvertures sédimentaires, manifestations, mécanismes, prospection. Mémoire BRGM, Orléans, pp. 129-141.

Barbanson, L., Touray, J.C., Saulas, D., Vadala P., 1983. Distribution à différentes échelles et chronologie relative des carbonates de l'Aptien de la Province de Santander: relation entre auréole ferrifère et minéralisations Zn-Pb du type Réocin. Chronique de la Recherche minière. 473, 39-48.

Borradaile, G.J., Tarling, D.H., 1981. The influence of deformation mechanisms on magnetic fabrics in weakly deformed rocks. Tectonophysics. 77, 151-168.

Bouillin, J.P., Bouchez, J.L., Lespinasse, P., Pecher, A., 1993. Granite emplacement in an extensional setting: an AMS study of the magmatic structures of Monte Capanne (Elba, Italy). Earth Planet. Sci. Lett. 118, 263-279.

De Wall, H., Warr, L.N., 2004. Oblique magnetic fabric in siderite-bearing pelitic rocks of the Upper Carboniferous Culm Basin, SW England: an indicator for paleo fluid migration?, in: Martin-Hernandez, F., Lüneburg, C., Aubourg, C., Jackson, M. (Eds.), Magnetic fabric: methods and applications. Geological Society of London, Special publications, pp. 493-507.

Dunlop, D.J., Özdemir, Ö., 1997. Rock magnetism: fundamentals and frontiers. Cambridge University Press, New York.

Evans, M.A., Lewchuk, M.T., Elmore, R.D., 2003. Strain partitioning of deformation mechanisms in limestones: examining the relationship of strain and Anisotropy of Magnetic Susceptibility (AMS). J. Struct. Geol. 25, 1525-1549.

Ferré, E.C., 2002. Theoretical models of intermediate and inverse AMS fabrics. Geophys. Res. Lett. 29, 10.1029/2001GL014367.

Grandia, F., Canals, A., Cardellach, E., Banks, D.A., Perona, J., 2003. Origin of ore-forming brines in sediment-hosted Zn-Pb deposits of the Basque-Cantabrian basin, Northern Spain. Econ. Geol.. 98, 1397-1411.

Heizmann, J.J., Laruelle, C., Vadon, A., 1988. Utilisation d'un détecteur courbe à localisation spatiale pour la mesure simultanée de plusieurs figures de pôles par les rayons X. Analusis. 16, 334-340.

Hejda, P., Kapicka, A., Petrovsky, E., Sjoberg, B., 1994. Analysis of hysteresis curves of samples with magnetite and hematite grains. IEEE transactions on magnetics. 30, 881-883.

Henry, B., Le Goff, M., 1995. Application de l'extension bivariate de la statistique Fisher aux données d'Anisotropie de Susceptibilité Magnétique: intégration des incertitudes de mesure sur l'orientation des directions principales. Acad. Sc. Paris. 320, 1037-1042.

Hounslow, M.W., 2001. The crystallographic fabric and texture of siderite in concretions: implications for siderite nucleation and growth processes. Sedimentology. 48, 533-557.

Hrouda, F., 1982. Magnetic anisotropy of rocks and its application in geology and geophysics. Geophys. Surv. 5, 37-82.

Hrouda, F., 1986. The effect of quartz on the magnetic anisotropy of quartzite. Studia geophys. geod. 30, 39-45.

Hrouda, F, 2004. Problems in interpreting ams parameters in diamagnetic rocks, in: Martín-Hernández, F., Lüneburg, C., Aubourg, C., M. Jackson, M. (Eds.), Magnetic fabric: methods and applications. Geological Society, London, Special Publications, 238, 49-59.

Hu, M.A., Disnar, J.R., Barbanson, L., Suarez-Ruiz, I., 1995. Hydrocarbon geochromatographic fractionation, water-washing, biodegradation and Zn-Pb ore genesis: the La Florida ore deposit (Spain), in: Grimalt, J.O., and Dorronsoro, C. (Eds.), Organic geochemistry: developments and application to energy, climate, environment and human history. A.I.G.O.A., Donastia-San Sebastian, pp. 1058-1060.

Hu, M.A., Disnar, J.R., Barbanson, L., Suarez-Ruiz, I., 1998. Processus d'altération thermique, physico-chimique et biologique des constituants organiques et genèse des minéralisations sulfurées: le gîte Zn-Pb de La Florida (Cantabria, Espagne). Can. J. Earth Sci. 35, 936-950.

Jelinek, V., 1981. Characterization of the magnetic fabric of rocks. Tectonophysics. 79, T63-T67.

Jover, O., Rochette, P., Lorand, J.P., Maeder, M., Bouchez, J.L., 1989. Magnetic mineralogy of some granites from the French Massif Central: origin of their low-field susceptibility. Phys. Earth Planet. Int. 55, 79-92.

Kessler, S.E., Stoiber, R.E., Billings, G.K., 1972. Direction of flow of mineralizing solutions at pine point, N.W.T. Econ. Geol. 67, 19-24.

Launeau, P., Robin, P.Y., 1996. Fabric analysis using the intercept method. Tectonophysics. 267, 91-119.

Nomade, S., Theveniaut, H., Chen, Y., Pouclet, A., Rigollet, C., 2000. Paleomagnetic study of French Guyana Early Jurassic dolerites: hypothesis of a multistage magmatic event. Earth Planet. Sci. Lett. 184, 155-168.

Nye, J.F., 1961. Propriétés physiques des cristaux. Dunod, Paris.

Owens, W.H., Rutter, E.H., 1978. The development of magnetic susceptibility anisotropy through crystallographic preferred orientation in a calcite rock. Phys. Earth Planet. Int. 16, 215-222.

Pascal, A., 1982. Evolution des systèmes biosédimentaires Urgoniens en Espagne du Nord. N. Jb. Päläont. Abh. 165,1, 77-86.

Pascal, A., 1984. Les systèmes biosédimentaire Urgoniens (Aptien-Albien) sur la marge nord-ibérique. Mémoire Géologique, Université de Dijon. 10, 651p.

Peters, C., Thompson, R., 1998. Magnetic identification of selected natural iron oxides and sulphides. Journal of Magnetism and Magnetic Materials. 183, 365-374.

Prieto, M., Paniagua, A., Marcos, C., 1996. Formation of primary inclusions under influence of the hydrodynamic environment. Eur. J. Mineral. 5, 987-996.

Rat, P., 1982. Subsidence et évolution des environnements sédimentaires sur la marge cantabrique (Espagne) du Crétacé. N. Jb. Päläont. Abh. 165, 1, 32-75.

Rat, P., Pascal, A., 1982. Les plates-formes carbonatées à Rudistes (dites urgoniennes) du Cretacé Inferieur et leur environnement. Cretaceous Res. 3, 155-166.

Rochette, P., 1988. Inverse magnetic fabric in carbonate bearing rocks. Earth Planet. Sci. Lett. 90, 229-237.

Rochette, P., Jackson, M., Aubourg, C., 1992. Rock magnetism and the interpretation of the anisotropy of magnetic susceptibility. Rev. Geophys. 30, 209-226.

Schmidt, V., Gunther, D., Hirt, A.M., 2006. Magnetic anisotropy of calcite at room-temperature. Tectonophysics. 418, 63-73.

Schneider, J., de Wall, H., Kontny, A., Bechstadt, T., 2004. Magnetic susceptibility variations in carbonates of the La Vid Group (Cantabrian zone, NW-Spain) related to burial diagenesis. Sediment. Geol. 166, 73-88.

Schulz, L., 1949a. A direct method of determining preferred orientation of a flat reflection sample using a Geiger counter X-ray spectrometer. J. Appl. Phys. 20, 1030-1033.

Schulz, L.G., 1949b. Determination of preferred orientation of flat transmission samples using a Geiger counter X-ray spectrometer. J. Appl. Phys. 20, 1033-1036.

Shogenova, A., 1999. The influence of dolomitization on the magnetic properties of Lower Palaeozoic carbonate rocks in Estonia, in: Tarling, D., Turner, P. (Eds.), Paleomagnetism and diagenesis in sediments. Geol. Soc., Special Publications, London, pp. 167-180.

Sizaret, S., Chen, Y., Barbanson, L., Henry, B., Camps, P., Marcoux, E., 2006a. Crystallization in flow—I. Palaeocirculation track by texture analysis and magnetic fabrics. Geophys. J. Int. 176, 605-612.

Sizaret, S., Chen, Y., Chauvet, A., Marcoux, E., Touray, J.C., 2003. Magnetic fabrics and fluid flow directions in hydrothermal systems. A case study in the Chaillac Ba-F-Fe deposits (France). Earth Planet. Sci. Lett. 206, 555-570.

Sizaret, S., Chen, Y., Marcoux, E., Touray, J.C., 2001. Anisotropy of Magnetic susceptibility (AMS) and trace chemistry: a new approach to discriminate between hydrothermal and supergene processes. Application to the Ba-Fe-F deposit of Chaillac (Indre, France). Comptes Rendus de l'Academie des Sciences - Series IIA - Earth and Planetary Science. 332, 431-437.

Sizaret, S., Fedioun, I., Barbanson, L., Chen, Y., 2006b. Crystallization in flow part II: modelling crystal growth kinetics controlled by boundary layer thickness. Geophys. J. Int. 176, 1027-1034.

Talbot, J.Y., Faure, M., Chen, Y., Martelet, G., 2005. Pull-apart emplacement of the Margeride granitic complex (French Massif Central). Implications for the late evolution of the Variscan orogen. J. Struct. Geol. 27, 1610-1629.

Tarling, D.H., Hrouda, F., 1993. The magnetic anisotropy of rocks. Chapman and Hall, London.

Velasco, F., Herrero, J.M., Yusta, I., Alonso, J.A., Seebold, I., Leach, D., 2003. Geology and geochemistry of the Reocin zinc-lead deposit, Basque-Cantabrian Basin, Northern Spain. Econ. geol. 98, 1371-1396.

Wing, B. A., Ferry, J.M., 2007. Magnitude and geometry of reactive fluid flow from direct inversion of spatial patterns of geochemical alteration. Am. J. Sci. 307, 793–832.

Yusta, I., Velasco, F., Herrero, J.M., 1998. Anomaly threshold estimation and data normalization using EDA statistics: application to lithogeochemical exploration in Lower Cretaceous Zn-Pb carbonate-hosted deposits, northern Spain. Appl. Geochem. 13, 421-439.

Table and figure captions

Table 1: AMS data and their associated parameters. L: limestone, D: dolomite host rock, FD: ferroan dolomite host rock, n: number of measured samples, P': corrected anisotropy degree, T: shape parameter (Jelinek, 1981), K_v: bulk susceptibility, D: declination, I: inclination, K_1, K_2, and K_3 are respectively the axes of the maximum, intermediate and minimum of magnetic susceptibility.

$$P' = \exp\left\{2\left[(\ln k_1 - \ln k_m)^2 + (\ln k_2 - \ln k_m)^2 + (\ln k_3 - \ln k_m)^2\right]\right\}^{1/2};\ \ln k_m = (\ln k_1 + \ln k_2 + \ln k_3)/3$$

$$P' = \exp\left\{2/9\left[(\ln(k_1/k_2) + \ln(k_1/k_3))^2 + (\ln(k_2/k_1) + \ln(k_2/k_3))^2 + (\ln(k_3/k_1) + \ln(k_3/k_2))^2\right]\right\}^{1/2}$$

$$T = \left[2\ln(k_2/k_3)/\ln(k_1/k_2)\right] - 1$$

Fig. 1: Simplified geological map of the Cretaceous basin containing La Florida mining district (taken of Yusta et al., 1998). The rectangle zone in NW shows approximately the studied area.

Fig. 2: (A) Geological section of La Florida mining district (after Barbanson et al., 1983). Dots show AMS sampling sites. L: limestone, D: dolomite host rock, FD: ferroan dolomite host rock. (B) Evolution of the general paragenetic sequence in La Florida mining district (after Barbanson & Touray, 1987).

Fig. 3: Lattice preferred orientation for the (0006) pole corresponding to ‹c› axes compared with the magnetic response of the studied samples. The greyscale present the pole

density of (h k i l). Measurements concern, dolomite (A and B) and Fe-rich dolomite (C and D). To facilitate comparison, projection was carried out in upper hemisphere for both data. (□: K_1, Δ: K_2, ○: K_3). Sample A (LFE-76b) come from site D_5 with K_v = 18.8 x 10^{-6} [SI], B (LFW-43) from D_2 with K_v = 18.58 x 10^{-6} [SI], C (LC-40) from FD_4 with K_v = 154.2 x 10^{-6} [SI] and D (LFE-45) come from FD_8 with K_v = 45 x 10^{-6} [SI]. K_v is the bulk susceptibility of the studied sample. The intervals of confidence at 95 per cent are not presented one the Figure because they are small than the symbols representing AMS ellipsoid axes.

Fig. 4: (A) SEM backscattered images from thin sections of ferroan dolomite host rock (sample LC-40); dark grey zones show the relics of initial dolomite grains whereas clear grey ones show zones enriched by iron; dotted lines outline the limits of single crystal grains, (B) average shape of the relics of initial dolomite (dark grey ribbons in A), (C) average distance between "nearest neighbours" of these relics, both obtained by SPO statistics (Launeau, and Robin, 1996). (D and E) SEM backscattered images from thin sections of dolomite host rock (sample LFW-43); dotted lines outline the limits of growth bands. K_1, K_2 and K_3 are respectively the maximum, intermediate and minimum semi axes of magnetic susceptibility ellipsoid.

Fig. 5: (A) Histogram of the bulk susceptibility for all samples of studied carbonates. (B) Graphic presentation of the shape parameter T according to the corrected anisotropy degree P' for all sites. (C) Graphic presentation of the corrected anisotropy degree P' vs. the bulk susceptibility for all samples of limestone.

Fig. 6: Isothermal Remanent Magnetization (IRM) acquisition curves of limestone (A), dolomite host rock (B), and ferroan dolomite host rock (C) ; and hysteresis loops of limestone (D), dolomite host rock (E), ferroan dolomite host rock (F). The samples

studied by IRM have K_v = -5.84 x 10^{-6} [SI] for limestone (sample LFW-6b, site L_3), K_v = 14.47 x 10^{-6} [SI] for dolomite host rock (LFE-20, D_4) and K_v = 120 x 10^{-6} [SI] for ferroan dolomite host rock (LFW-29, FD_2). Those measured by hysteresis method have K_v = -4.46 x 10^{-6} [SI] for limestone (LFW-3, L_3), K_v = 6.20 x 10^{-6} [SI] for dolomite host rock (LFE-83b, D_5) and K_v = 111 x 10^{-6} [SI] for ferroan dolomite host rock (LFW-30, FD_2).

Fig. 7: Stereogram comparing the principal axes (■ : K_1, ▲ : K_2 and ● : K_3) of ARM (grey) and AMS (black), the circles give the interval of confidence at 95 per cent. Samples of limestone (sample LFE-84b, site L_{10}), dolomite host rock (LFW-45, D_2), and ferroan dolomite host rock (LFW-38a FD_3) have respectively the following volumetric susceptibilities: -1.02 x 10^{-6} [SI], 18.77 x 10^{-6} [SI] and 160.3 x 10^{-6} [SI]. Projection was carried out in lower hemisphere in tilt-corrected coordinates.

Fig. 8: AMS responses for sites of ferroan dolomite host rock (A) and limestone/dolomite host rock (B). Average orientations of the principal axes were calculated with bivariate statistics (Henry and Le Goff, 1995). ■, ▲ and ● correspond to K_1, K_2 and K_3, respectively. Magnetic foliation is defined by the K_1 – K_2 plane, and the magnetic lineation corresponds to the K_1 axis. Projection was carried out in lower hemisphere in tilt-corrected coordinates. Curves around poles correspond to the interval of confidence at 95 per cent.

Fig. 9: Block-diagram showing the principal direction of the fluid flow and that of sediments transport suggested by AMS results from this study.

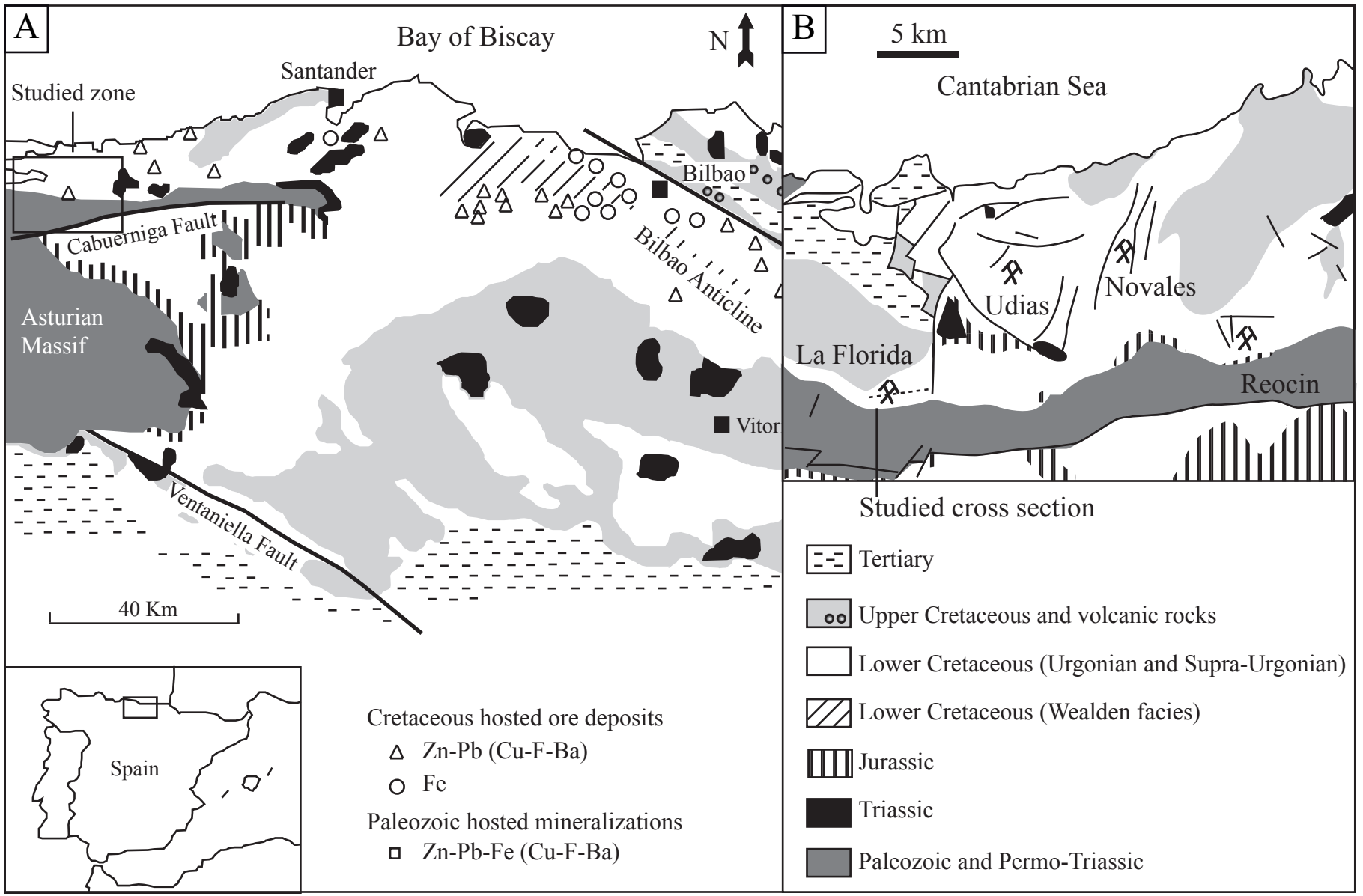
A
Bay of Biscay
N
Santander
Studied zone
Bilbao
Cabuerniga Fault
Bilbao Anticline
Asturian
Massif
Vitor
Ventaniella Fault
40 Km
Spain
Cretaceous hosted ore deposits
Zn-Pb (Cu-F-Ba)
Fe
Paleozoic hosted mineralizations
Zn-Pb-Fe (Cu-F-Ba)
B
5 km
Cantabrian Sea
Udias
Novales
La Florida
Reocin
Studied cross section
Tertiary
Upper Cretaceous and volcanic rocks
Lower Cretaceous (Urgonian and Supra-Urgonian)
Lower Cretaceous (Wealden facies)
Jurassic
Triassic
Paleozoic and Permo-Triassic

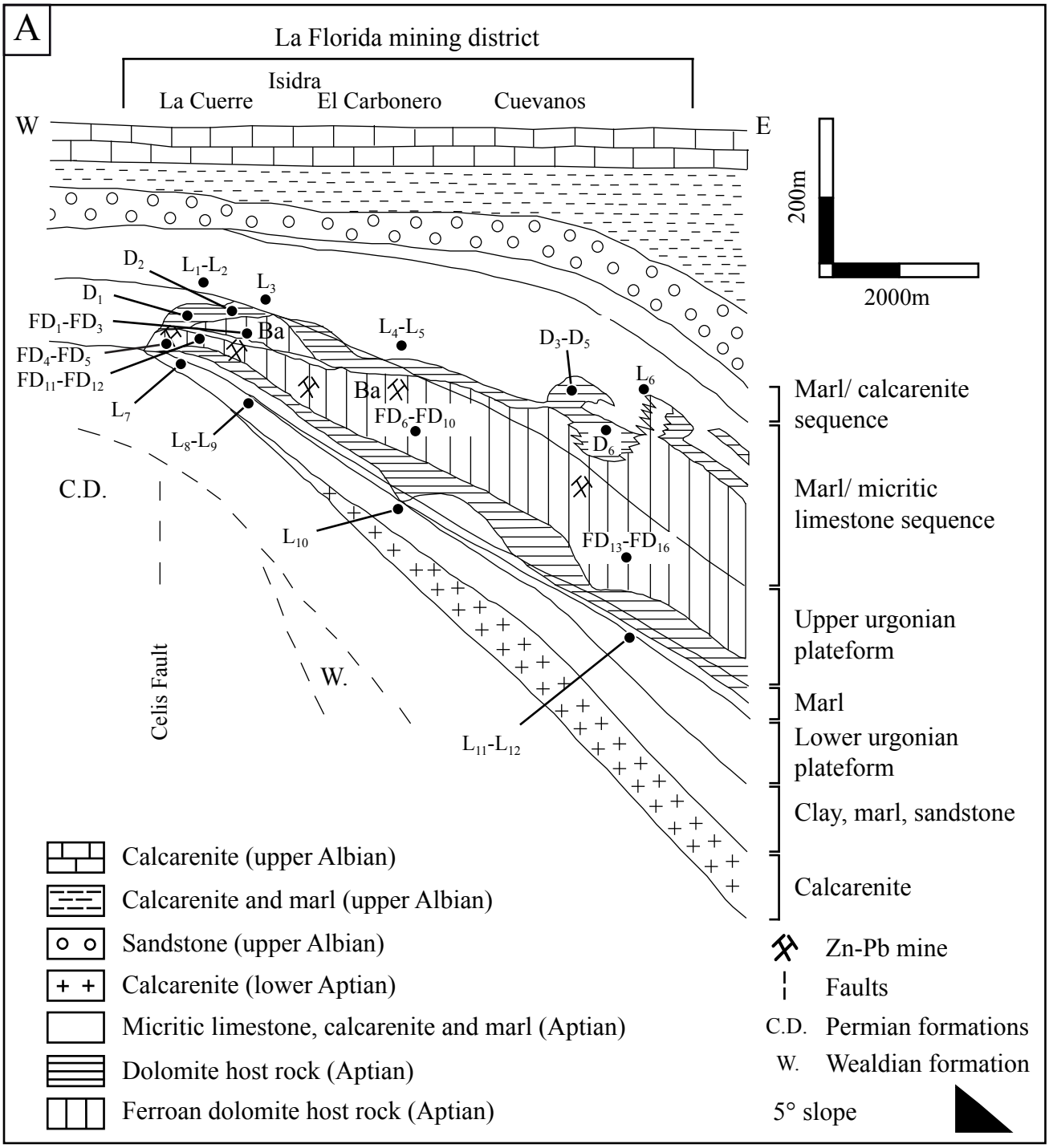
A
La Florida mining district
Isidra
La Cuerre
El Carbonero
Cuevanos
W
E
200m
2000m
D2
L1-L2
L3
D1
FD1-FD3
Ba
L4-L5
D3-D5
L6
FD4-FD5
FD11-FD12
L7
L8-L9
Ba
FD6-FD10
D6
C.D.
L10
FD13-FD16
Celis Fault
W.
L11-L12
Marl/ calcarenite sequence
Marl/ micritic limestone sequence
Upper urgonian plateform
Marl
Lower urgonian plateform
Clay, marl, sandstone
Calcarenite
Calcarenite (upper Albian)
Calcarenite and marl (upper Albian)
Sandstone (upper Albian)
Calcarenite (lower Aptian)
Micritic limestone, calcarenite and marl (Aptian)
Dolomite host rock (Aptian)
Ferroan dolomite host rock (Aptian)
Zn-Pb mine
Faults
C.D. Permian formations
W. Wealdian formation
5° slope

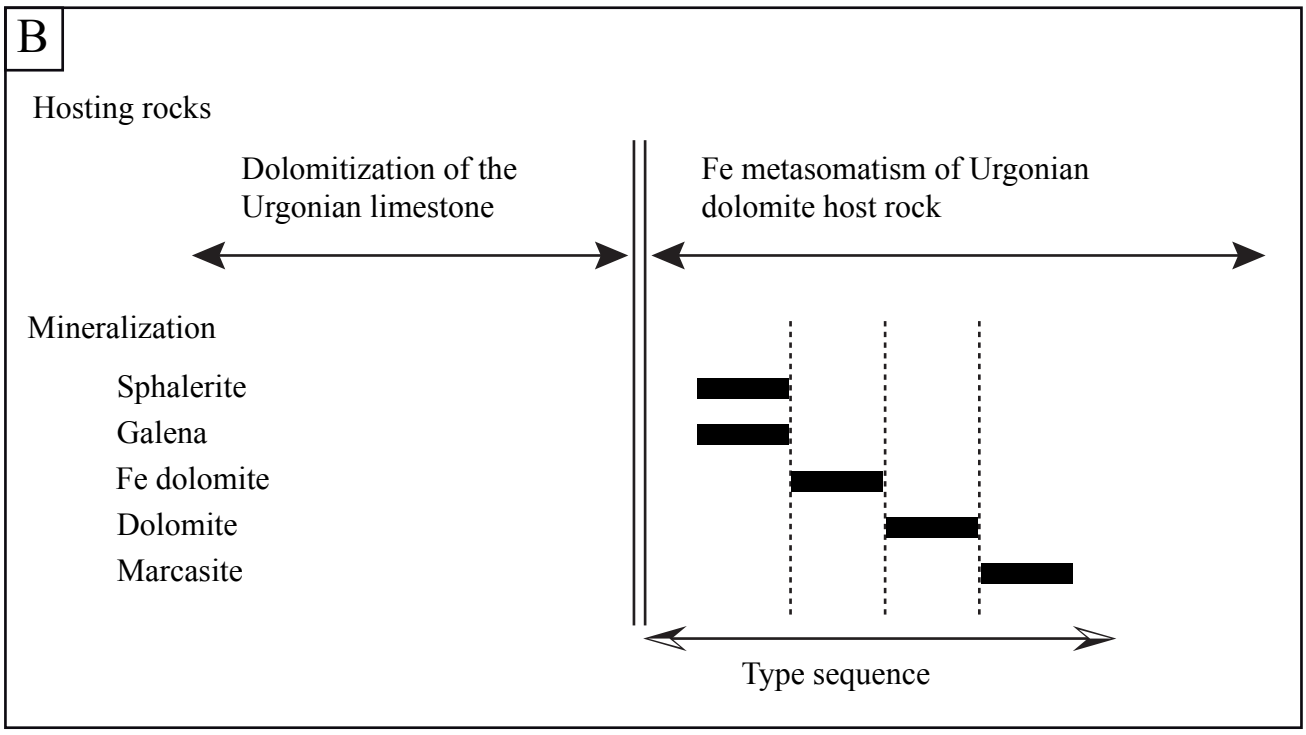
B
Hosting rocks
Dolomitization of the Urgonian limestone
Fe metasomatism of Urgonian dolomite host rock
Mineralization
Sphalerite
Galena
Fe dolomite
Dolomite
Marcasite
Type sequence

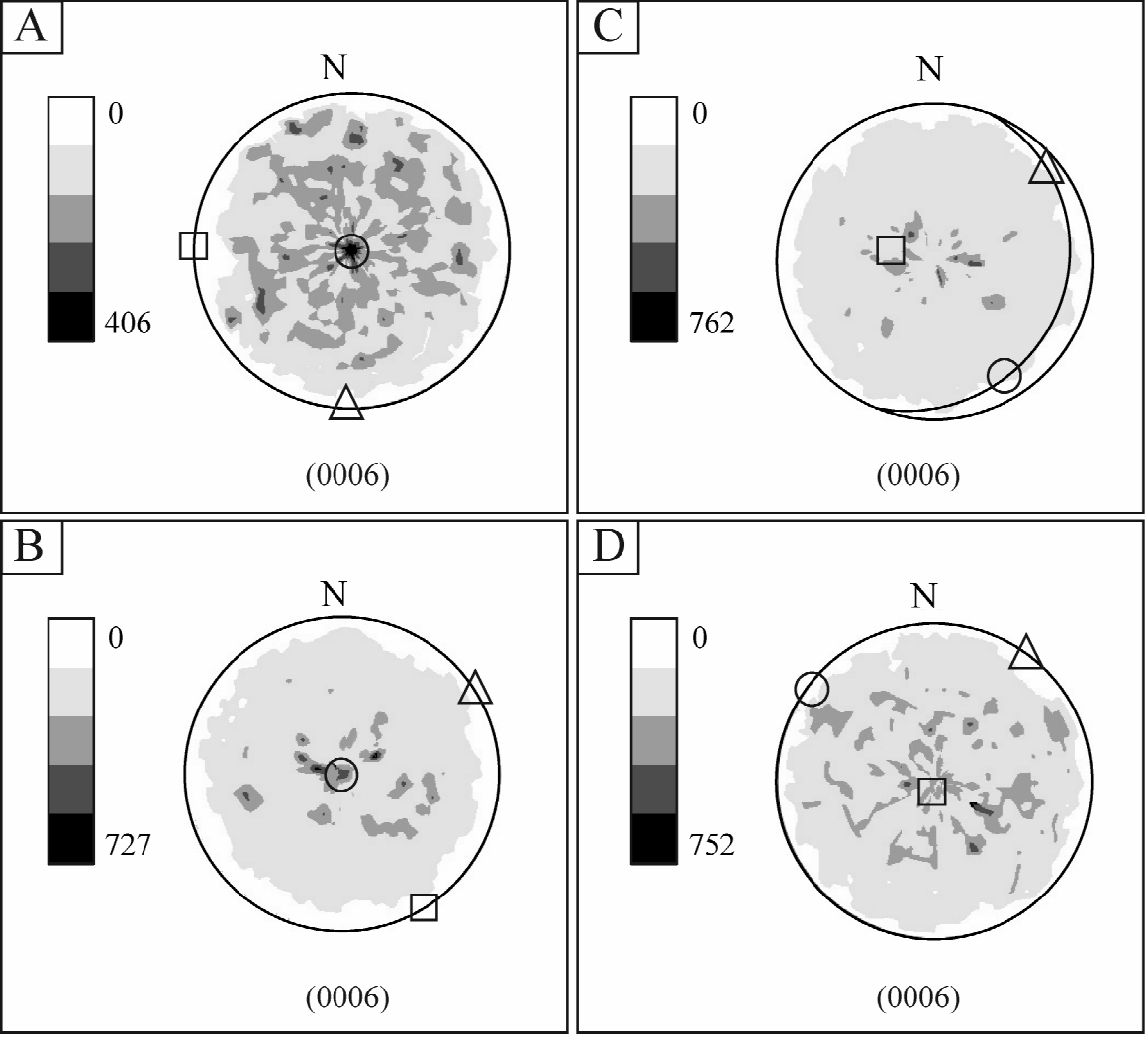
A
N
0
406
(0006)
C
N
0
762
(0006)
B
N
0
727
(0006)
D
N
0
752
(0006)

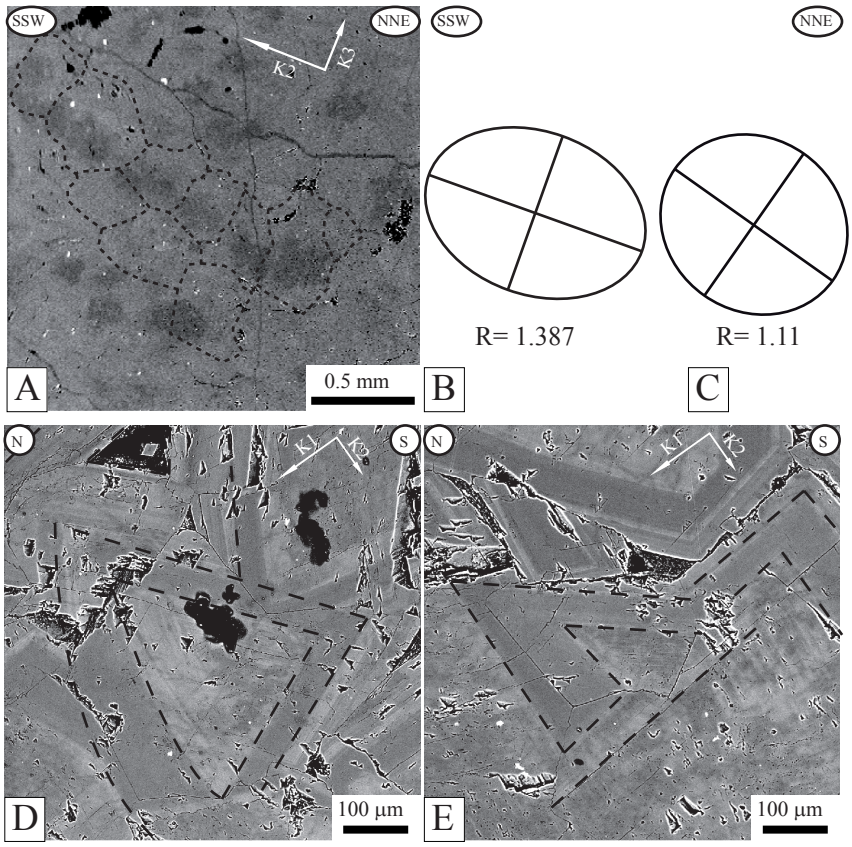
SSW
NNE
K2
K3
0.5 mm
A
SSW
NNE
R= 1.387
R= 1.11
B
C
N
S
K1
K3
100 µm
D
N
S
K1
K3
100 µm
E

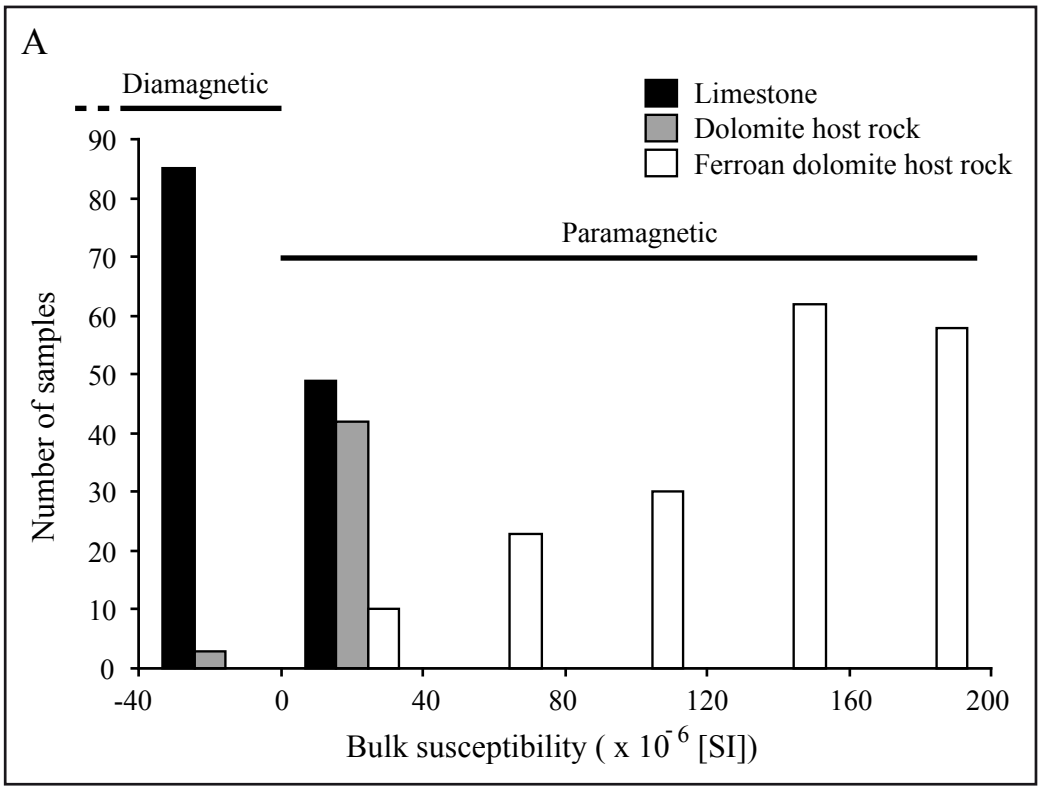
A
Diamagnetic
Paramagnetic
Limestone
Dolomite host rock
Ferroan dolomite host rock
Number of samples
Bulk susceptibility (x 10-6 [SI])

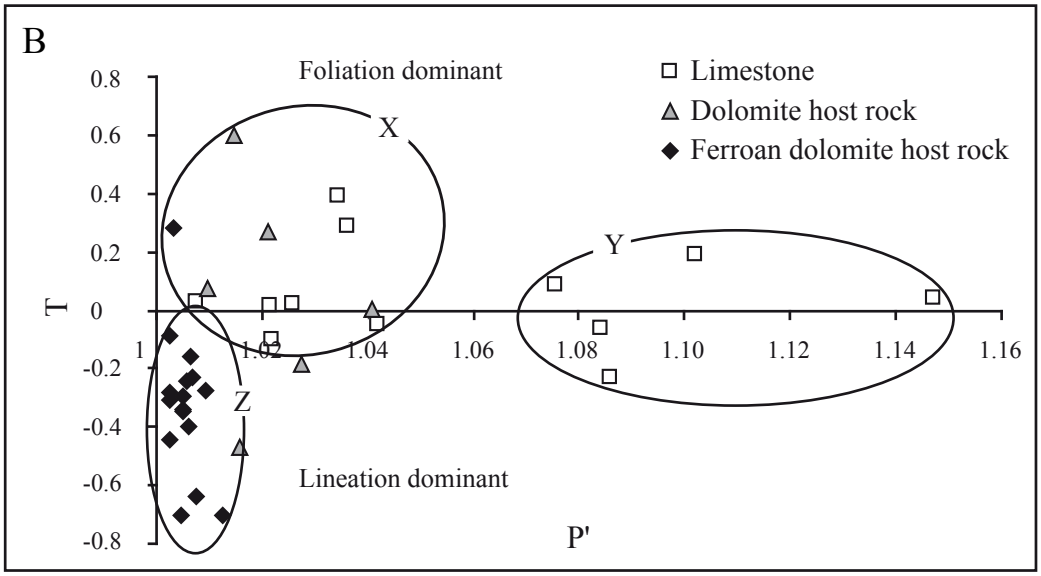
B
Foliation dominant
Lineation dominant
X
Y
Z
Limestone
Dolomite host rock
Ferroan dolomite host rock
T
P'

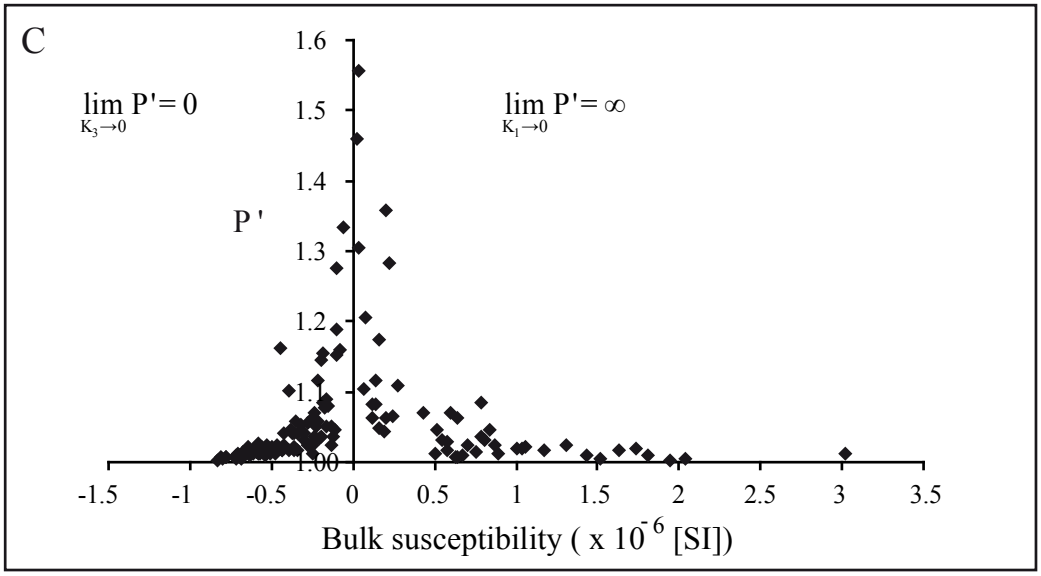
C
lim P'= 0
K3→0
lim P'= ∞
K1→0
P '
Bulk susceptibility (x 10-6 [SI])

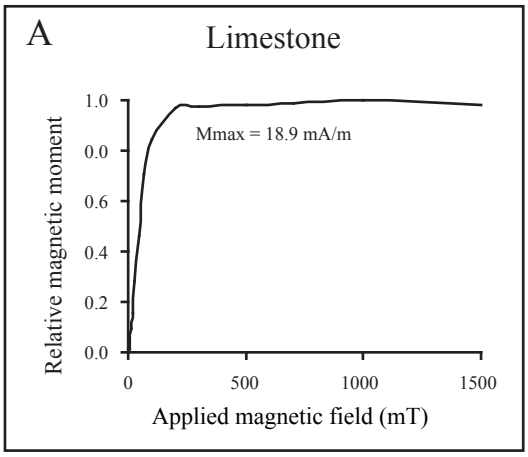
A
Limestone
Mmax = 18.9 mA/m
Relative magnetic moment
1.0
0.0
0.6
0.4
0.2
0.0
0
500
1000
1500
Applied magnetic field (mT)

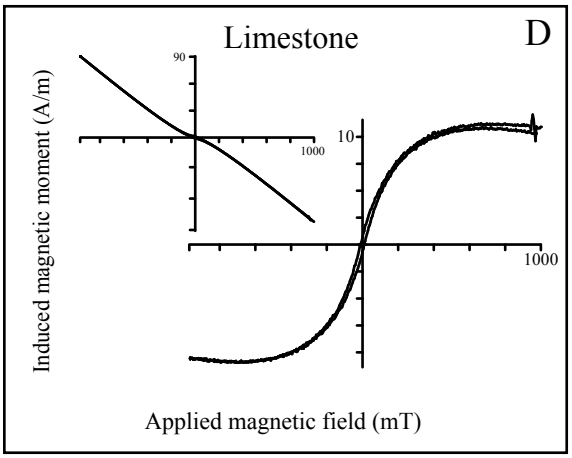
Limestone
D
Induced magnetic moment (A/m)
90
1000
10
1000
Applied magnetic field (mT)

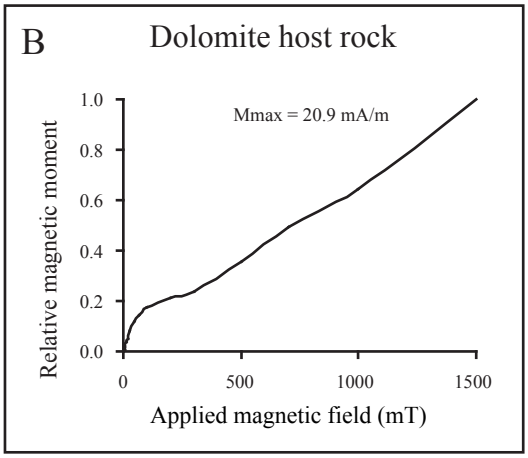
B
Dolomite host rock
Mmax = 20.9 mA/m
Relative magnetic moment
1.0
0.8
0.6
0.4
0.2
0.0
0
500
1000
1500
Applied magnetic field (mT)

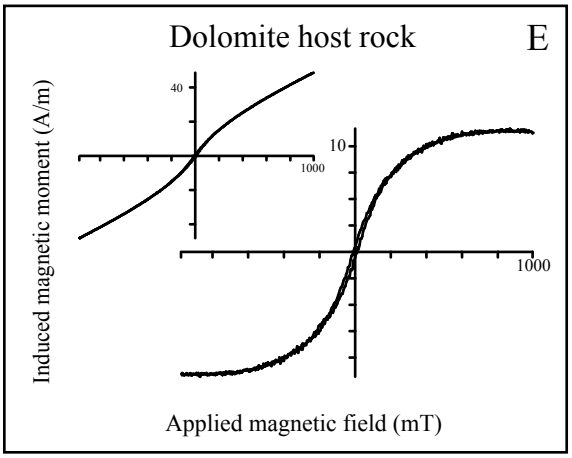
Dolomite host rock
E
Induced magnetic moment (A/m)
40
1000
10
1000
Applied magnetic field (mT)

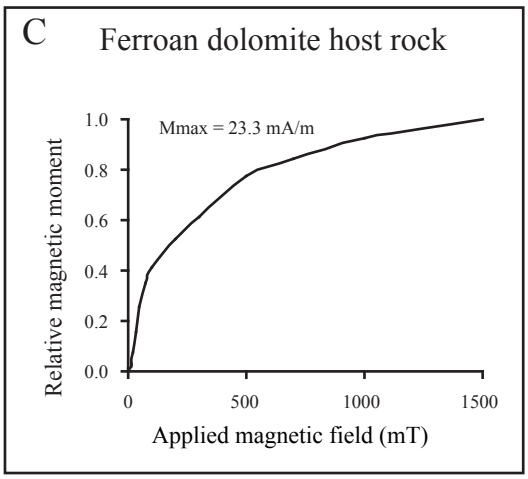
C
Ferroan dolomite host rock
Mmax = 23.3 mA/m
Relative magnetic moment
1.0
0.8
0.6
0.4
0.2
0.0
0
500
1000
1500
Applied magnetic field (mT)

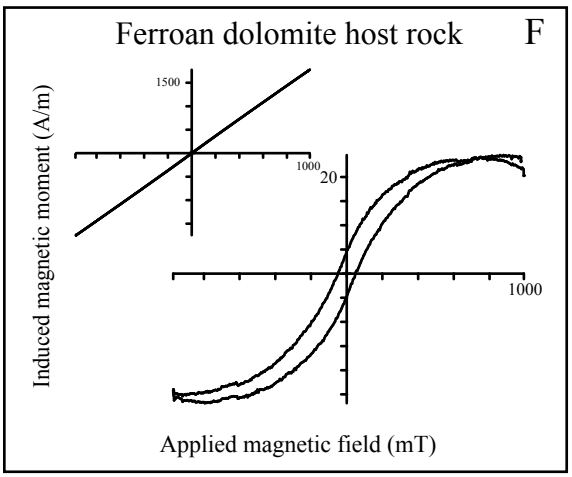
Ferroan dolomite host rock
F
Induced magnetic moment (A/m)
1500
1000
20
1000
Applied magnetic field (mT)

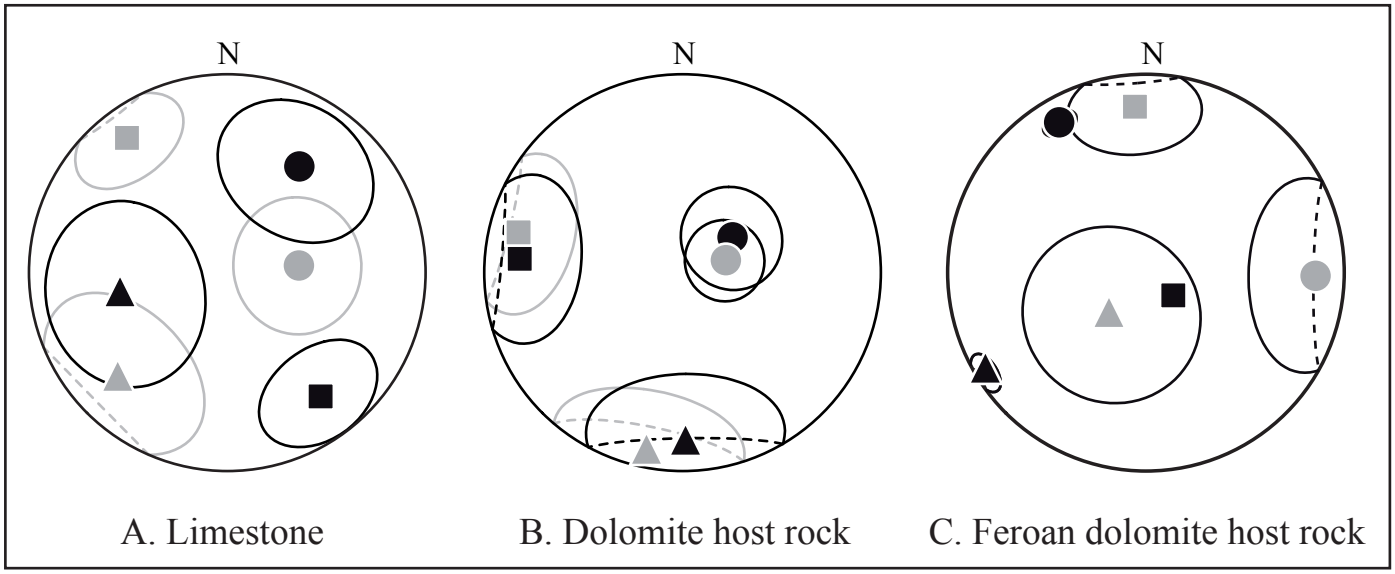
N
N
N
A. Limestone
B. Dolomite host rock
C. Feroan dolomite host rock

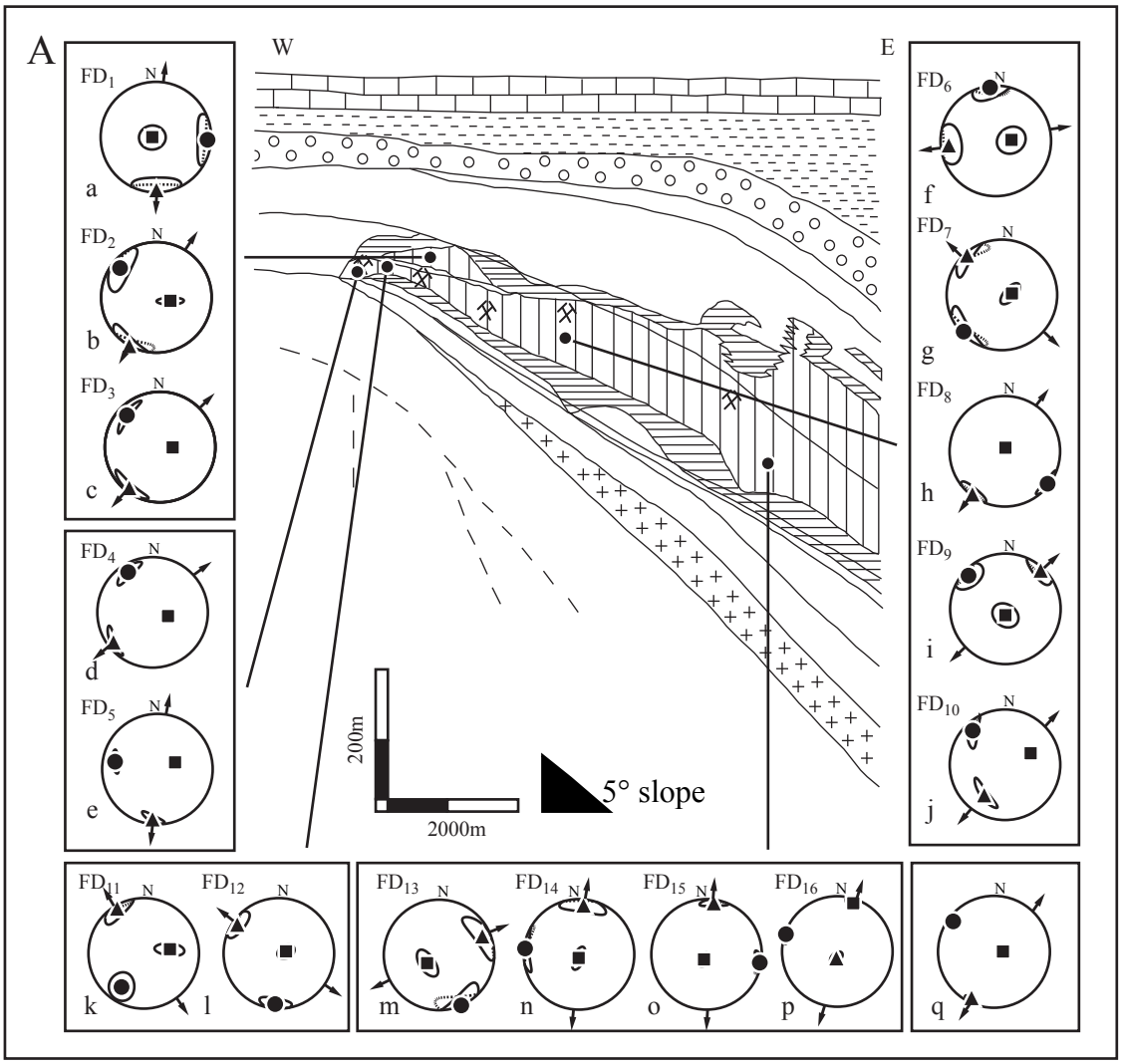
A
W
E
FD1
FD2
FD3
FD4
FD5
FD6
FD7
FD8
FD9
FD10
FD11
FD12
FD13
FD14
FD15
FD16
N
a
b
c
d
e
f
g
h
i
j
k
l
m
n
o
p
q
200m
2000m
5° slope

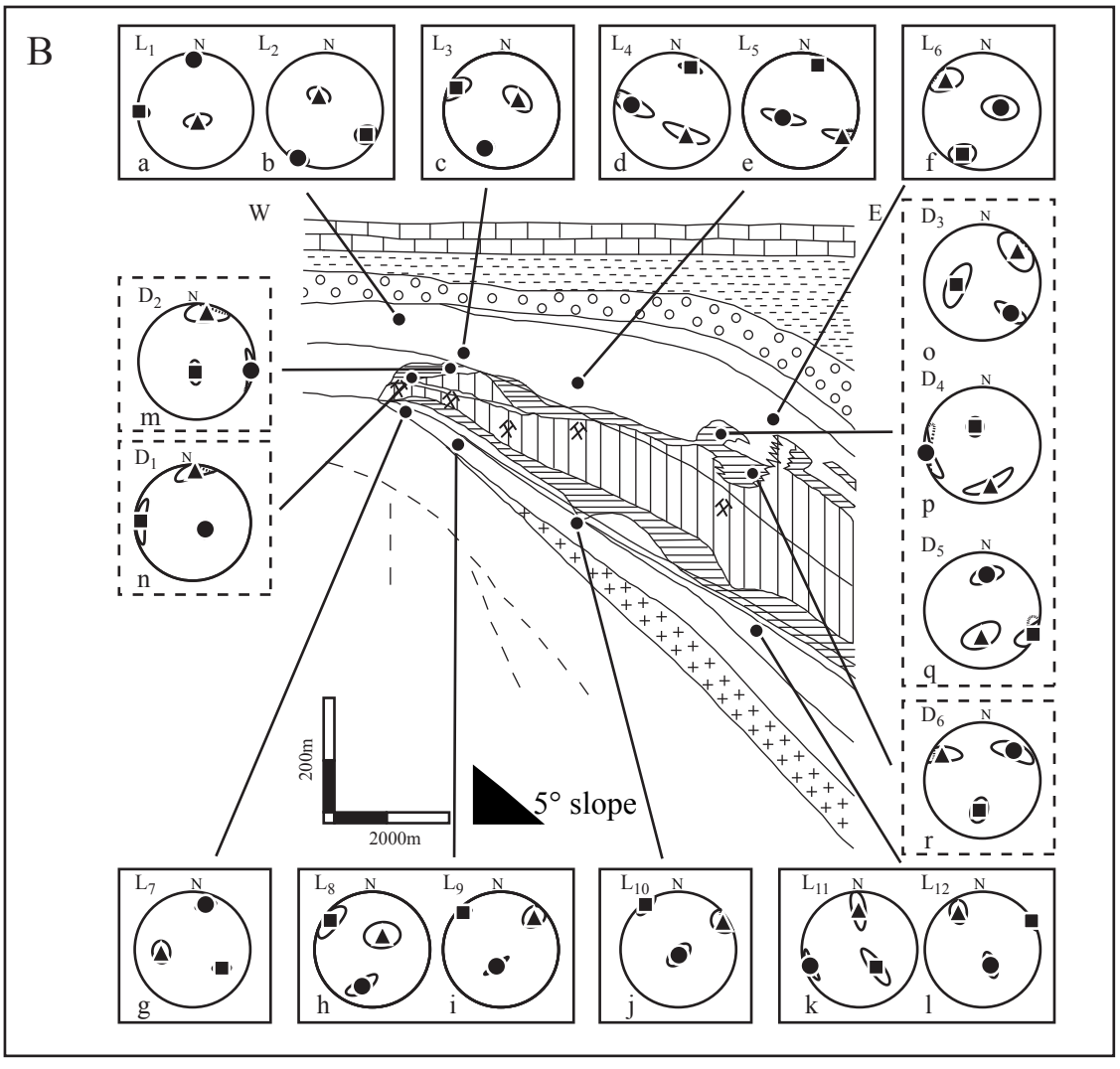
B
W
E
L1
L2
L3
L4
L5
L6
L7
L8
L9
L10
L11
L12
D1
D2
D3
D4
D5
D6
N
a
b
c
d
e
f
g
h
i
j
k
l
m
n
o
p
q
r
200m
2000m
5° slope

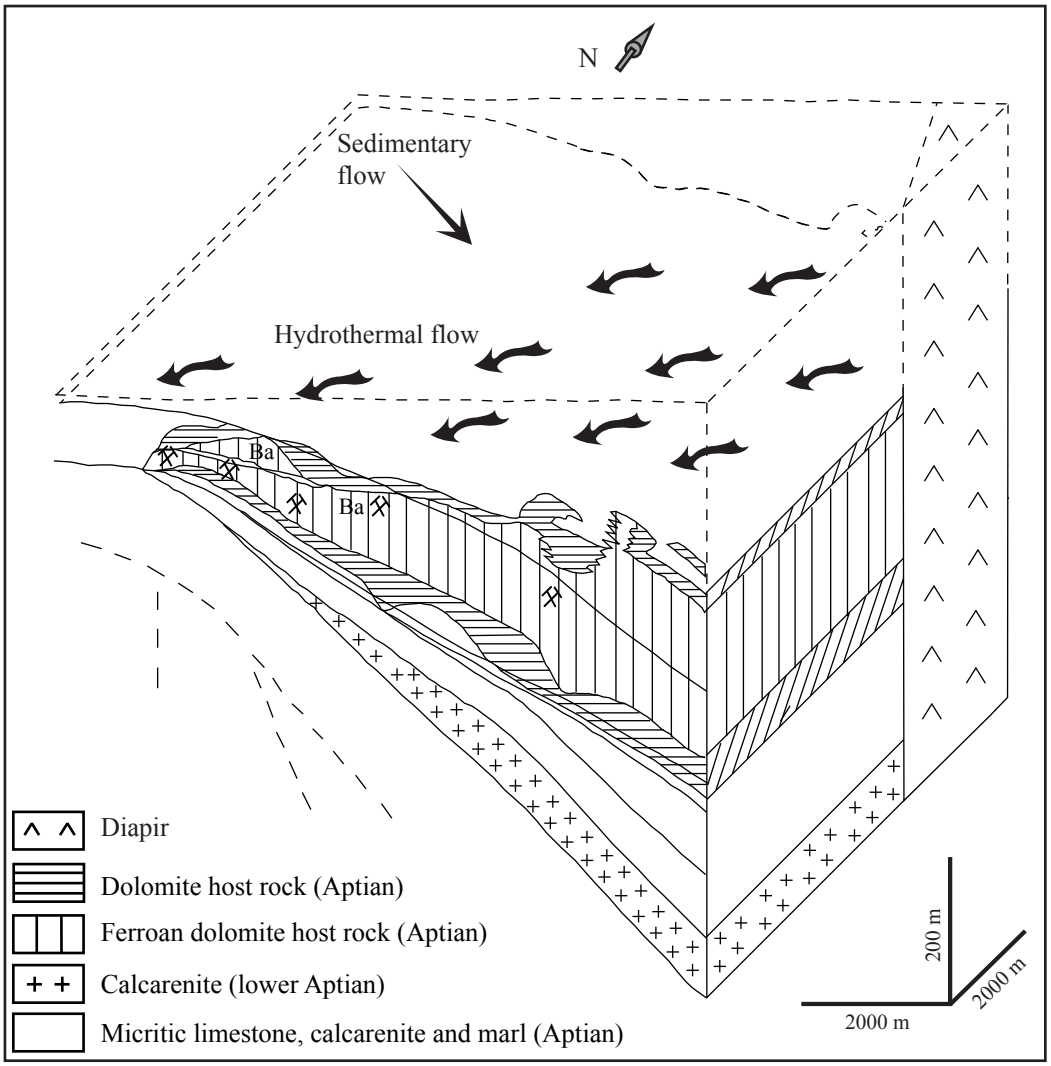
N
Sedimentary flow
Hydrothermal flow
Ba
Ba
Diapir
Dolomite host rock (Aptian)
Ferroan dolomite host rock (Aptian)
Calcarenite (lower Aptian)
Micritic limestone, calcarenite and marl (Aptian)
200 m
2000 m
2000 m

						K_1		K_2		K_3	
Site	Rock	n	P'	T	K.10^{-6} SI	D (°)	I (°)	D (°)	I (°)	D (°)	I (°)
L1	L	12	1.022	-0.098	-4.5	269	3	168	75	358	13
L2	L	26	1.026	0.02	0.2	121	18	338	67	210	6
L3	L	14	1.084	-0.062	0.8	296	14	54	61	204	29
L4	L	6	1.035	0.394	-4.0	24	20	149	50	279	30
L5	L	5	1.021	0.019	-4.6	21	18	121	17	249	63
L6	L	10	1.008	0.048	-7.3	200	15	326	11	56	80
L7	L	14	1.147	0.04	-1.5	123	39	265	45	16	20
L8	L	9	1.042	-0.049	-3.9	304	13	35	65	196	34
L9	L	10	1.086	-0.231	1.2	314	10	45	20	195	66
L10	L	16	1.102	0.191	5.3	324	5	58	10	175	82
L11	L	5	1.076	0.085	5.9	137	55	359	31	252	11
L12	L	7	1.036	0.291	10.1	60	3	327	23	153	65
D1	D	9	1.027	-0.192	6.0	187	75	12	13	99	5
D2	D	10	1.015	0.602	21.2	272	11	3	10	117	70
D3	D	7	1.041	0.005	11.1	264	53	48	20	138	28
D4	D	6	1.01	0.073	8.7	338	61	169	30	262	2
D5	D	9	1.021	0.232	8.5	115	3	182	53	7	39
D6	D	5	1.016	-0.472	17.7	186	47	303	18	47	27
FD1	FD	11	1.006	-0.245	139.4	263	85	179	6	93	7
FD2	FD	6	1.005	-0.294	122.6	105	69	210	1	309	17
FD3	FD	11	1.007	-0.64	154.7	93	72	218	9	314	18
FD4	FD	17	1.006	-0.402	107.4	105	66	233	13	329	16
FD5	FD	11	1.012	-0.704	158.7	70	62	186	11	280	23
FD6	FD	8	1.002	-0.282	129.1	88	67	266	16	354	3
FD7	FD	6	1.003	-0.446	112.1	82	78	318	2	227	2
FD8	FD	6	1.005	-0.342	78.7	10	85	218	4	127	3
FD9	FD	9	1.003	-0.087	140.4	180	80	42	5	312	11
FD10	FD	4	1.005	-0.337	81.4	66	48	215	35	317	16
FD11	FD	11	1.002	-0.308	139.2	82	50	329	8	213	28
FD12	FD	27	1.007	-0.233	82.8	80	79	305	9	184	9
FD13	FD	4	1.005	-0.704	84.7	235	68	66	15	156	0
FD14	FD	5	1.009	-0.276	159.0	184	84	5	11	276	2
FD15	FD	5	1.007	-0.16	146.3	206	81	8	6	99	3
FD16	FD	6	1.003	0.285	52.2	18	9	189	81	289	2